AGROCIENCIA URUGUAY

Agrociencia Uruguay 2026 | Volume 30 | Article e1750
DOI: 10.31285/AGRO.30.1750
ISSN 2730-5066

Paleocurrent Analysis of the Piedras de Afilar Formation (Neoproterozoic, Uruguay): Paleoenvironmental and Paleogeographic Implications

Pamoukaghlián, K. [1]; Gaucher, C. [1]; Poiré, D. [2]

[1] *Universidad de la República, Facultad de Ciencias, Instituto de Ciencias Geológicas, Montevideo, Uruguay*

[2] *Universidad Nacional de La Plata, Facultad de Ciencias Naturales y Museo, Centro de Investigaciones Geológicas, La Plata, Argentina*

Editor

Leticia Chiglino
Universidad de la República, Centro Universitario Regional Este (CURE), Treinta y Tres, Uruguay

Received *6 May 2025*
Accepted *29 Sep 2026*
Published *10 Nov 2026*

Correspondence

Karina Pamoukaghlián
kpamoukaghlian@fcien.edu.uy

Abstract

A detailed paleocurrent analysis was carried out in the outcrop area of the Piedras de Afilar Formation, which is a sedimentary succession corresponding to a shallow marine platform. With the aim of analyzing paleocurrents and their importance in basin analysis, a survey at the outcrop level was carried out. Paleocurrents measured in interference ripple marks suggest a NW-SE paleo-shoreline. Flute cast paleocurrents with directions towards NE and measured paleocurrents in Cuchilla Alta, in planar cross-stratification and trough cross-stratification (bimodal to oblique patterns to the NE and SE), suggest a provenance from the west. A rotation in the paleocurrent direction due to deformation was observed, which required a systematic correction. Considering this, a regional drag fold is interpreted as a sinistral shear sense indicator for the Sarandí del Yi Shear Zone reactivation. Regionally, the Arroyo del Soldado Group presents paleocurrent directions mainly to the east, similar to the Piedras de Afilar Formation. This suggests a provenance from the west for the mentioned Neoproterozoic units, which is confirmed by the detrital zircon ages, with Mesoproterozoic ages, interpreted as a provenance from a proto-Andean belt of the Río de la Plata Craton, counterpart of the Grenvillian in Laurentia.

Keywords: sedimentary basin analysis, Paleogeography, Sarandí del Yi Shear Zone, Grenville Orogen

CC BY

Pamoukaghlián, K., Gaucher, C., & Poiré, D. (2026). Paleocurrent analysis of the Piedras de Afilar Formation (Neoproterozoic, Uruguay): Paleoenvironmental and paleogeographic implications. *Agrociencia Uruguay, 30*, Article e1750. https://doi.org/10.31285/AGRO.30.1750

Análisis de paleocorrientes de la Formación Piedras de Afilar (Neoproterozoico de Uruguay): implicancias de paleoambiente, paleogeografía y proveniencia

Resumen

Un detallado análisis de paleocorrientes fue llevado a cabo en el área de afloramiento de la Formación Piedras de Afilar, una sucesión sedimentaria que corresponde a un paleoambiente de plataforma marino somero. Con el objetivo de analizar las paleocorrientes y su importancia en el análisis de cuencas, se desarrolló una observación a nivel de afloramiento. Las paleocorrientes medidas en ripples de interferencia sugieren una línea de paleocosta NW-SE. Las paleocorrientes de calcos de flujo con sentido hacia el NE y las medidas de paleocorrientes en Cuchilla Alta, en estratificación cruzada planar y en estratificación cruzada en artesa (patrones bimodales a oblicuos hacia el NE y SE), sugieren una proveniencia desde el oeste. Se observó una rotación en la dirección de las paleocorrientes debida a la deformación, que requirió una corrección sistemática. Teniendo esto en cuenta, se interpreta un pliegue de arrastre regional como un megaindicador sinestral de la reactivación de la Zona de Cizalla Sarandí del Yi. Regionalmente, el Grupo Arroyo del Soldado presenta direcciones de paleocorrientes principalmente hacia el este, tal como la Formación Piedras de Afilar. Esto sugiere una proveniencia desde el oeste de las mencionadas unidades Neoproterozoicas, lo cual es confirmado por las edades de los zircones detríticos, con edades mesoproterozoicas interpretadas como una proveniencia de un cinturón protoandino del Cratón del Río de la Plata, contraparte del Grenviliano en Laurentia.

Palabras clave: análisis de cuencas sedimentarias, paleogeografía, Zona de Cizalla Sarandí del Yi, orógeno Grenville

Análise de paleocorrentes da Formação Piedras de Afilar: Implicações no paleoambiente, paleogeografia e proveniência

Resumo

Uma análise detalhada de paleocorrentes foi realizada na área de afloramento da Formação Piedras de Afilar, que é uma sucessão sedimentar que corresponde a um paleoambiente de plataforma marinha rasa. Com o objetivo de analisar as paleocorrentes e sua importância na análise de bacias, foi desenvolvida uma observação em escala de afloramento. Paleocorrentes medidas em ondulações de interferência sugerem uma linha paleocosta NW-SE. As paleocorrentes dos *flute casts* com sentido para NE e as medições de paleocorrentes em Cuchilla Alta, na estratificação cruzada planar e na estratificação cruzada acanalada (padrões bimodais a oblíquos em direção ao NE e SE) sugerem uma procedência do oeste. Foi observada uma rotação na direção das paleocorrentes devido a deformação subsequente, o que exigiu uma correção sistemática. Tendo isto em conta, uma dobra de arrasto regional é interpretada como um megaindicador sinestral da reativação da Zona de Cisalhamento de Sarandí del Yi. Regionalmente, o Grupo Arroyo del Soldado apresenta direções paleocorrentes principalmente para leste, similar a Formação Piedras de Afilar. Isto sugere uma proveniência do oeste das referidas unidades Neoproterozóicas, o que é confirmado pelas idades dos zircões detríticos, com idades mesoproterozóicas interpretadas como proveniência de um cinturão proto-andino do Cráton Río de la Plata, homólogo do Grenviliano em Laurentia.

Palavras-chave: análise de bacias sedimentares, Paleogeografía, Zona de Cisalhamento de Sarandí del Yi, Orógeno Grenville

1. Introduction

The Piedras de Afilar Formation (PAFm) (Jones, 1956) is a Neoproterozoic sedimentary cover of the Río de la Plata Craton (RPC), where mineralogical (Cingolani et al., 1990) and lithostratigraphic (Bossi & Navarro, 1991) studies have been conducted. U-Pb ages of detrital zircons (U-Pb ICP-LA-MS) in the PAFm revealed dominant Mesoproterozoic zircon populations (62%), with age peaks at 1487, 1347, 1242, and 1009 Ma, which did not match the underlying basement ages (Gaucher et al., 2008). Only 37% of zircons presented Paleoproterozoic ages between 2005-2068 Ma and 1779-1876 Ma, which coincide with the ages of the basement, the Tandilia

Terrane of the RPC (Bossi & Cingolani, 2009; Pamoukaghlián et al., 2017). These results, combined with others from correlative units in Argentina, indicated a provenance area located on the western edge of the RPC. This positive area corresponds to a "recycled orogen" which could be a proto-Andean margin associated with a Grenvillian orogen and its counterpart in South America, the Sunsas Belt (Chernicoff et al., 2012; Cingolani, 2011; Finney & Gaucher, 2022; Gaucher et al., 2008, 2009, 2011; Santos et al., 2003, 2017).

A detailed facies analysis and a detailed paleoenvironmental reconstruction of the PAFm have been presented by (Pamoukaghlián, 2012; Pamoukaghlián et al., 2021). On this basis, the present study provides a paleocurrent analysis of the PAFm, focusing mainly on the psammitic facies of the Cuchilla Alta Member, for the interpretation of the paleoenvironmental, paleogeographic and provenance aspects, as part of the results of the first author's doctoral thesis, including an update and reinterpretation of the results. It is essential for provenance studies to integrate paleocurrent data with petrographic analyses (Pamoukaghlián et al., 2021), detrital zircon ages (Finney & Gaucher, 2022; Gaucher et al., 2008), and Sm-Nd ages (Pamoukaghlián, 2012; Pamoukaghlián et al., 2017).

It is important to note that, although it is not the main objective of this study, adequate sedimentological and stratigraphic analyses are very important for groundwater exploration. The sandstones of the PAFm constitute porous and fractured aquifers. Given their high cementation and consolidation, they behave as poor porous aquifers and, in some cases, as good fractured aquifers, especially in areas where there are evident tectonic discontinuities. The spatial characterization of the orientation of the sandstone bodies and the spatial distribution of the permeable detrital facies make it possible to define the primary anisotropy of the porous medium. The detailed understanding of the architecture of fluvial channels and coastlines provides a fundamental predictive conceptual model to optimize the studies of groundwater resources and local hydrogeological flows.

Groundwater exploration and exploitation in the area are currently limited. Consequently, substantial yields are sometimes obtained, whereas elsewhere wells have very low or even zero yields. This problem is typical of heterogeneous environments and deserves a more in-depth study.

2. Geological Context

Four Precambrian terranes are recognized in the basement of Uruguay (Bossi & Cingolani, 2009; Bossi & Piñeyro, 2014; Bossi et al., 1998), as shown in Figure 1. The Piedra Alta Terrane (Bossi et al., 1993; Santos et al., 2003) is made up of two orogenic belts and granite-gneissic complexes, corresponding to the Transamazonian orogeny (2.150-2000 Ma; Bossi & Cingolani, 2009; Pamoukaghlián et al., 2017; Santos et al., 2003). The Sarandí del Yi Shear Zone separates the Piedra Alta and Tandilia terranes to the west, from the Nico Pérez Terrane to the east; the latter comprising rocks of complex evolution, ranging in age from Archaean to Neoproterozoic (Gaucher, 2000; Gaucher et al., 2008, 2011; Hartmann et al., 2001). The Sierra Ballena Shear Zone separates the Nico Pérez Terrane from the Cuchilla Dionisio Terrane (Bossi & Gaucher, 2004; Bossi et al., 2005; Gaucher et al., 2009; Lenz et al., 2011; Will et al., 2019). The PAFm is a Neoproterozoic cover of the Tandilia Terrane (Bossi et al., 2005), as shown in Figure 1. The northern boundary of the Tandilia Terrane was recognized as the Colonia Shear Zone (Abre et al., 2014; Bossi et al., 2005; Ribot et al., 2005), which separates the Tandilia Terrane to the south from the Piedra Alta Terrane to the north (Bossi & Cingolani, 2009). The basement of the Tandilia Terrane in Uruguay consists of a Paleoproterozoic metasedimentary succession (Montevideo Formation), metamorphosed during the Transamazonian orogeny and intruded by granites between 2.17 and 2.05 Ga (Basei et al., 2016; Oyhantçabal et al., 1998, 2003; Santos et al., 2003). The La Paz Granite is the only known Neoproterozoic intrusion in the Tandilia Terrane, with U-Pb ages in zircon between 585 ± 4 and 564 ± 4 Ma (Abre et al., 2014 & Will et al., 2023, respectively). This terrane continues in Argentina, cropping out extensively in the Tandilia area (Buenos Aires Province), origin of its name (Bossi & Cingolani, 2009).

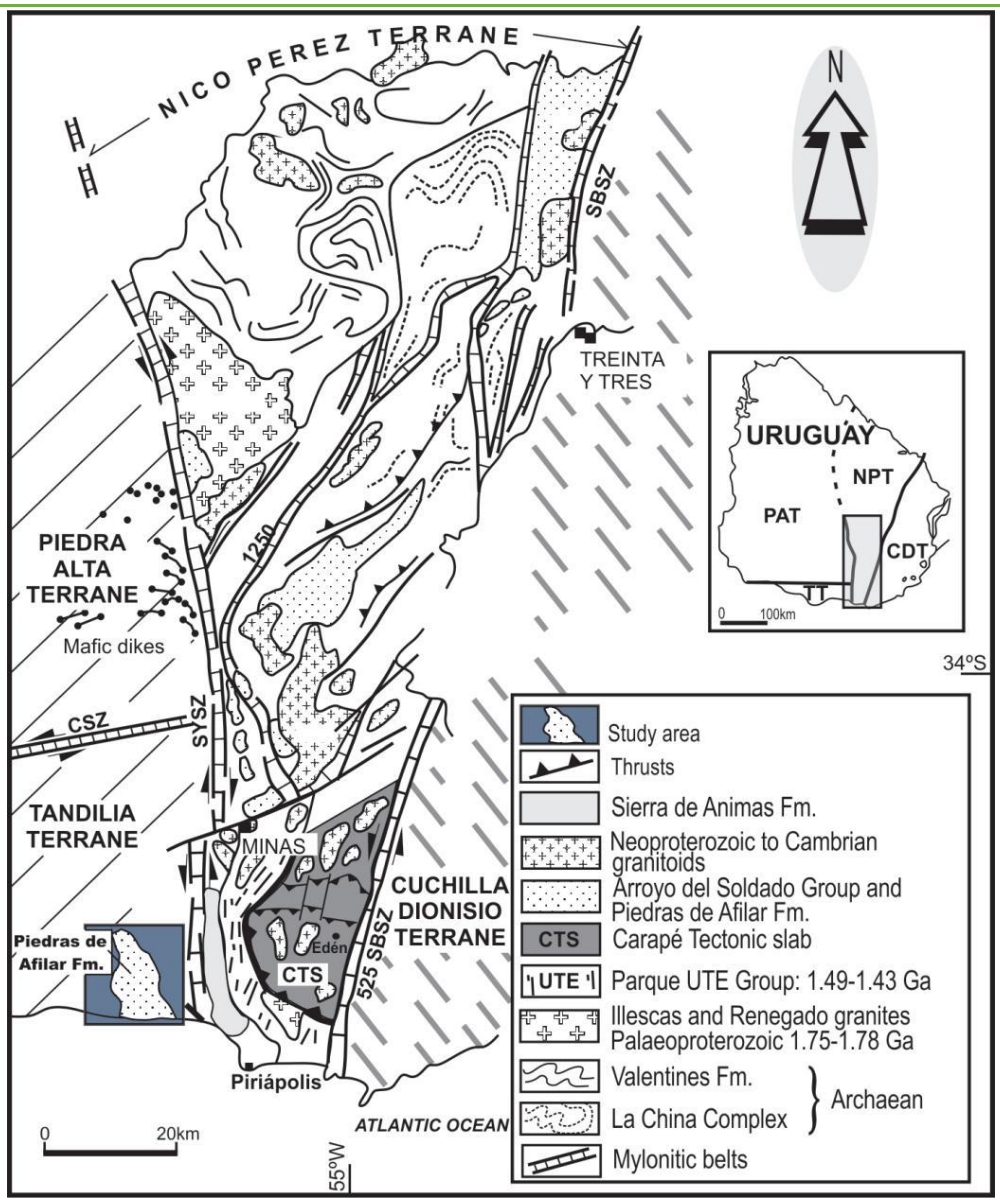


Figure 1. Tectonostratigraphic setting, showing the location of the Piedras de Afilar Formation

CSZ: Colonia Shear Zone, SYSZ: Sarandí del Yi Shear Zone, SBSZ: Sierra Ballena Shear Zone.

2.1 Basement of the Piedras de Afilar Formation

In the study area, the Piedras de Afilar Formation occurs as a sedimentary relict that unconformably overlies the Paleoproterozoic basement, which is part of the Tandilia Terrane (Bossi & Piñeyro, 2014). Three units were recognized as part of the PAFm basement in the area:

(1) The Montevideo Formation, of Paleoproterozoic age (Pando Belt), previously studied by Walther (1948), Bossi et al. (1998), and Oyhantçabal et al. (2003), among others. Metasedimentary rocks include micaschists containing muscovite, biotite, almandine garnet, staurolite, andalusite, plagioclase, and quartz. In its type area the Montevideo Formation includes ortho-amphibolites with pillow-lava structures, dated at ca. 2,200 Ma by whole-rock K-Ar (Oyhantçabal et al., 2003; Preciozzi et al., 1999).

(2) Soca Granite, a rapakivi granite that has an alkaline composition and is composed of quartz, microcline, plagioclase, biotite, zircon, apatite, allanite, and titanite (Oyhantçabal et al., 1998). It was dated by U-Pb SHRIMP in zircons interpreting a crystallization age of 2054 ± 6 Ma (Santos et al., 2003). Well-developed wiborgitic textures occur in several parts of the pluton (Abre et al., 2014).

(3) Coronilla granite (Jones, 1956; Spoturno et al., 2004), a fine-grained alkali-feldspar granite, composed of quartz, microcline, orthoclase, plagioclase, and micas. A Paleoproterozoic age is suggested for this pluton, but no radiometric data are available (Spoturno et al., 2004).

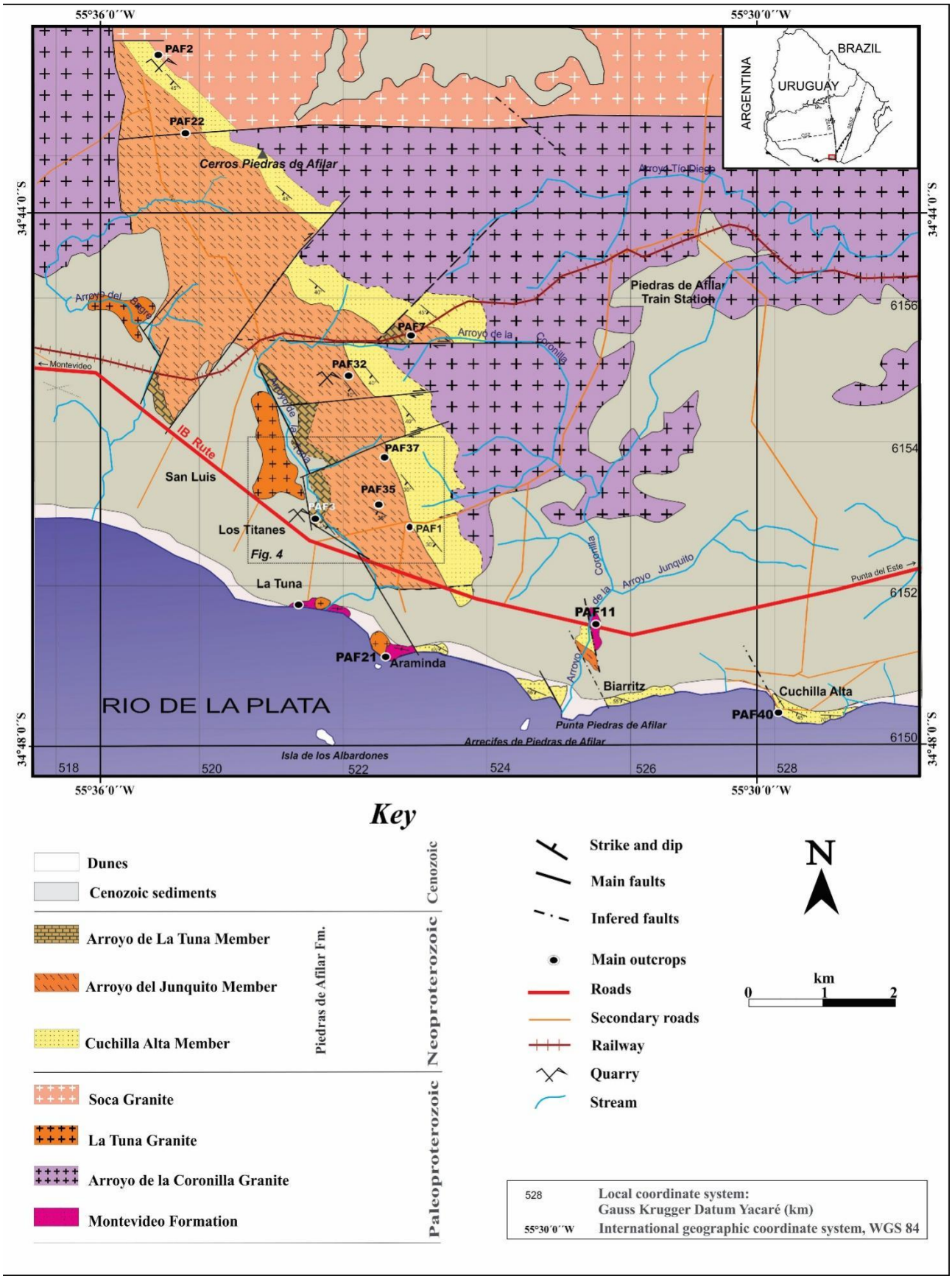


Figure 2. Geological map of the Piedras de Afilar Formation, showing the main outcrops and sampling points

The La Tuna Granite was considered to intrude the Neoproterozoic sequence of PAFm and was assigned a Cambrian age (Spoturno et al., 2004). However, subsequent studies demonstrated that both the granite and its host metaquartzites are of Paleoproterozoic age and that La Tuna Granite has a U-Pb LA-ICP-MS zircon age of 2156 ± 26 Ma, while the host metaquartzites were assigned to the Montevideo Formation (Pamoukaghlián et al., 2017).

The contact of the PAFm with the Paleoproterozoic basement is well exposed in the north of the study area in the González Quarry (PAF2, Figure 2), where the Soca Granite is overlain by the PAFm in an erosional unconformity (Gaucher et al., 2008; Pamoukaghlián, 2012). To the south, the PAFm rocks overlie schists containing chiastolite from the Montevideo Formation, with angular and erosional unconformity (PAF11, Figure 2).

2.2 Piedras de Afilar Formation

The PAFm, which crops out in the southeast of the Canelones Department, was defined by Jones (1956), who described this succession as composed of sandstones, pelites, and limestones, with its type area in the Piedras de Afilar Hills (Figure 2). More recently, this formation was divided into three members, which are described below (Figure 3; Pamoukaghlián, 2012; Pamoukaghlián et al., 2010, 2014, 2021).

The *Cuchilla Alta Member* crops out as a NW-directed belt. The type area is in Cuchilla Alta (site PAF40, Figure 2), and its stratotype is defined in the González Quarry (site PAF2, Figure 2). Its main characteristics are as follows: (a) it overlies the Paleoproterozoic basement with an erosional unconformity and conformably underlies the pelites of the Arroyo del Junquito Member; (b) it is a fining and thinning-upward sequence approximately 200 to 400 m thick; (c) the sandstones are mainly quartz-arenites and subarkoses, with subordinate siltstones that are intercalated with the sandstones; (d) it exhibits abundant sedimentary structures (see Figure 4), such as symmetrical and asymmetrical ripples, interference ripple marks, flute casts, parting lineation, convolute bedding, planar and trough cross-stratification, hummocky and megahummocky cross-stratification (Pamoukaghlián, 2012; Pamoukaghlián et al., 2014, 2021).

The *Arroyo del Junquito Member* is composed of shales and siltstones, which overlie the sandstones of the Cuchilla Alta Member (Figure 3). Its stratotype is located 1 km south of the Imhoff Quarry (point PAF32, Figure 2). The main characteristics of the Arroyo del Junquito Member are: (a) it transitionally overlies the *Cuchilla Alta Member*; (b) it is slightly more than 50 m thick; (c) the typical paragenesis of dark pelites is quartz + illite + kaolinite + chlorite + chlorite/smectite; (d) green and red pelites also occur; (e) dolerite intrusions are very frequent in this member, producing epidote-hornfels (Pamoukaghlián et al., 2021). No fossils have been recognized despite several palynological macerations (Gaucher, 2000; Pamoukaghlián, 2012); those reported by Pecoits et al. (2008) have been regarded as dubio- or pseudofossils (Pamoukaghlián, 2012; Poiré & Gaucher, 2009).

The *Arroyo de la Tuna Member* at the top is made up of carbonate rocks (Figure 3). Dark gray limestones and marls are observed, interbedded with black pelites and dolerite sills. Its stratotype was defined at the Heide Quarry (site PAF3, Figure 2). This member is characterized by: (a) limestones and marls interbedded with pelites; (b) scarce outcrops with thicknesses of only 10 m; (c) it conformably overlies the Arroyo del Junquito Member and represents the top of the PAFm (Pamoukaghlián, 2012; Pamoukaghlián et al., 2021).

Dolerites intrude the entire sequence (Figure 3), especially the pelites of the Arroyo del Junquito Member, and are mapped together with the PAFm due to their close spatial relationship. Two types of textures are observed: microgranular subophitic and granular pseudolamprophyric textures (Coronel et al., 1982). K-Ar ages of 382 ± 11 Ma have been reported for these dolerites (Cingolani et al., 1990). However, other authors have proposed an age of 739 ± 19 Ma for dolerites, based on detrital clays (Dristas et al., 2023), suggesting that this would be a minimum age for the Piedras de Afilar Formation, although this is contradictory to other data mentioned below.

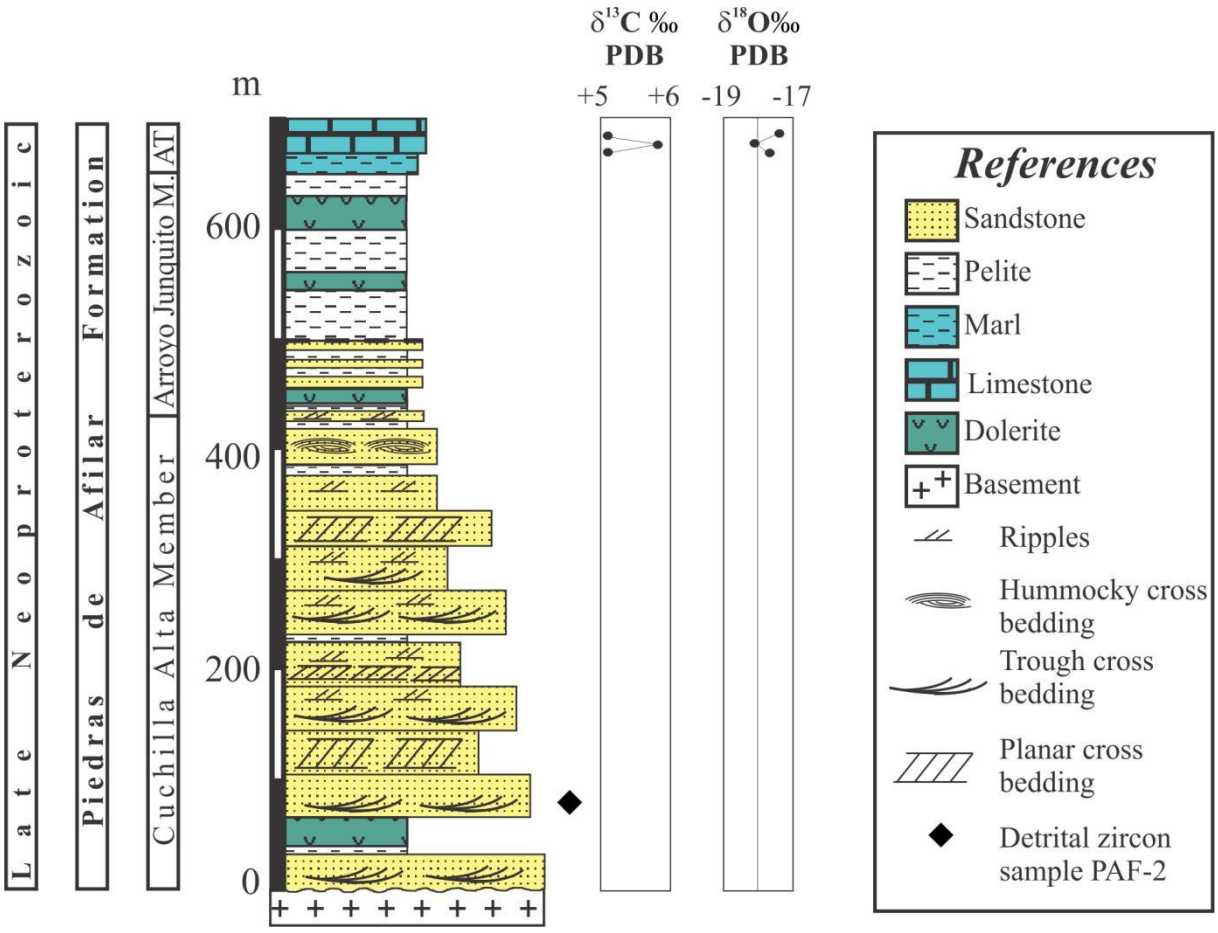


Figure 3. Synthetic stratigraphic column of the Piedras de Afilar Formation

Source. Adapted from Poiré and Gaucher (2009).

The PAFm has been considered Neoproterozoic in age (Bossi et al., 1998; Pamoukaghlián et al., 2006), despite the lack of fossils or precise radiometric data that could constrain its age. Given the maximum age provided by the age of the youngest detrital zircon of 962 ± 19 Ma and the youngest zircon population of 1008 Ma (Finney & Gaucher, 2022; Gaucher et al., 2008), the PAFm must have been deposited in the Neoproterozoic since the unit was affected by the Brasiliano orogeny, which affected the entire eastern margin of the Rio de la Plata Craton during the late Ediacaran (Bossi & Navarro, 1991; Lenz et al., 2011; Oyhantçabal et al., 2011; Pamoukaghlián et al., 2006). Recently, Gaucher et al. (2026) reported a U-Pb age of 601 ± 8 Ma for a dolerite sill cross-cutting the PAFm. This age is identical, within analytical uncertainty, to K-Ar ages obtained from sericite of the host rock in contact with dolerites, which yielded ages of 604±6 Ma and 609±10 Ma (Dristas et al., 2023). Finally, positive values of $\delta^{13}C$ between 5.1 and 5.8 ‰ VPDB were obtained for the limestones of the Arroyo de la Tuna Member (Pamoukaghlián, 2012; Pamoukaghlián et al., 2006) (Figure 3), which are common in the Cryogenian and Ediacaran rocks (Halverson et al., 2005).

The PAFm has been correlated with the Cerro Largo, Olavarría, and lower Loma Negra formations, of the Sierras Bayas Group (Tandilia Terrane, Argentina; Pamoukaghlián, 2012; Pamoukaghlián et al., 2021; Poiré & Gaucher, 2009), based on a similar, deepening-upward sequence that culminates in a carbonate ramp, a comparable depositional environment with a similar zircon age distribution (Cingolani, 2011; Gaucher et al., 2008) and positive $\delta^{13}C$ values for basal carbonate units (Arrouy et al., 2019; Gómez-Peral et al., 2017, 2018). These units have been assigned to the Ediacaran based on biostratigraphic data (Arrouy et al., 2019; Gaucher et al., 2005; Pamoukaghlián, 2012).

On the other hand, the PAFm has also been correlated with the Yerbal and Polanco formations of the Arroyo del Soldado Group in the Nico Pérez Terrane (Cingolani, 2011; Cingolani et al., 1990; Pamoukaghlián et al., 2014), which present maximum ages given by the youngest zircon of 664 ± 11 Ma, as well as biostratigraphic data suggesting an Ediacaran age (Gaucher, 2014, 2018; Gaucher & Sprechmann, 1999; Gaucher et al., 2003; Pamoukaghlián, 2012). Therefore, all evidence suggests a Neoproterozoic, and probably early Ediacaran, depositional age for the PAFm.

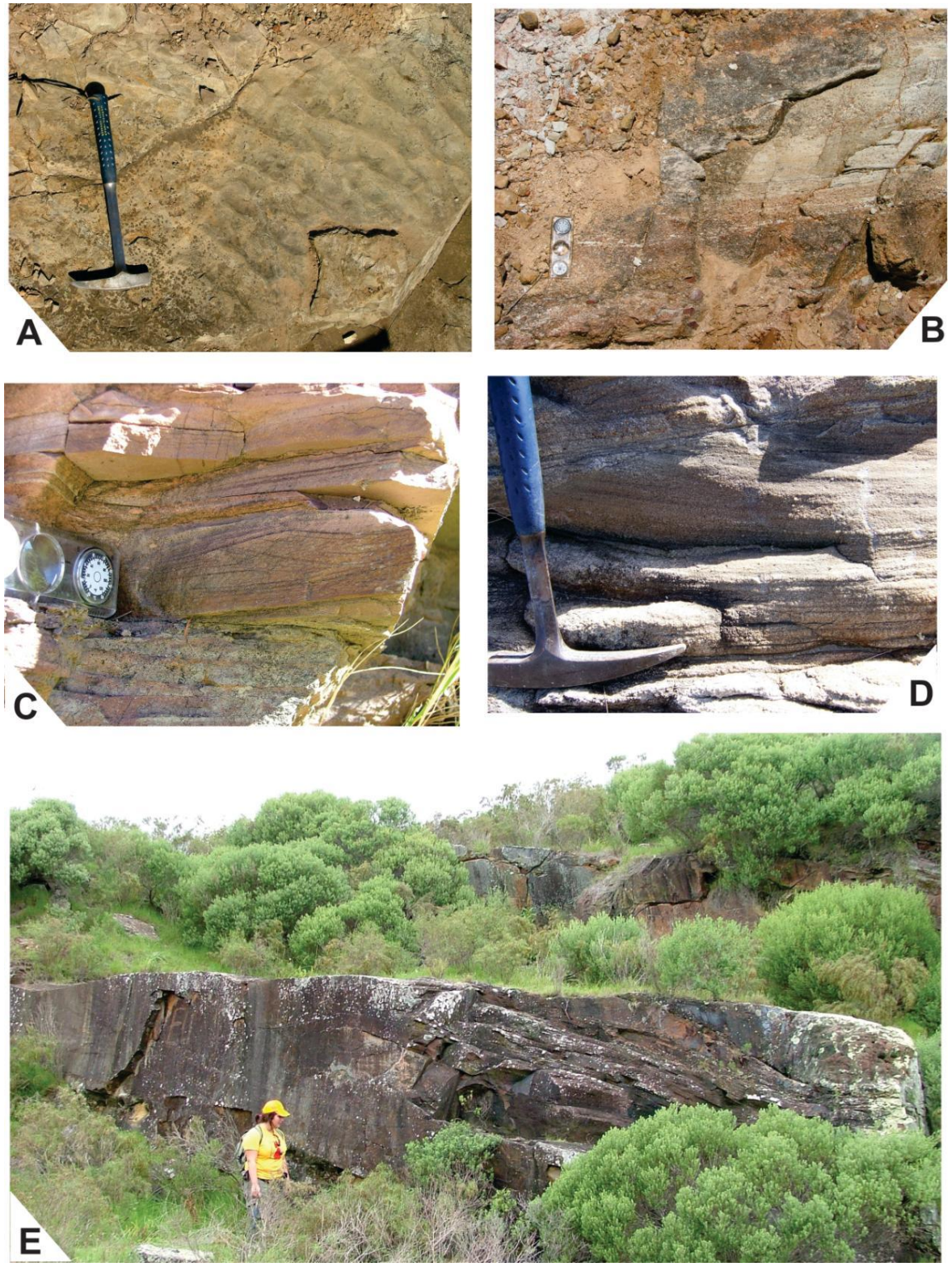


Figure 4. Main sedimentary structures where paleocurrents were measured: (A) interference ripple marks in quartzarenites, indicating two perpendicular paleocurrent directions; (B) partition lineation; (C) hummocky cross-stratification at Cuchilla Alta; (D) trough cross-stratification at Cuchilla Alta; (E) megahummocky cross-stratification in sandstones at the Imhoff Quarry

3. Materials and Methods

The following methodology was applied according to the type and arrangement of the sedimentary structures, based partly on a modified and updated version of the first author's doctoral thesis (Pamoukaghlián, 2012):

(1) At fieldwork, paleocurrents were measured at the mesoscale (outcrop scale) in unidirectional structures, such as asymmetric ripples and cross-stratification, and in bidirectional structures (symmetrical ripples and mega-ripples). Regarding the trough cross-stratification, a large sample of measurements was taken in locations where these structures are extensively exposed and display a three-dimensional geometry (53 measurements in Cuchilla Alta; Pamoukaghlián, 2012). When three-dimensional exposure was not observed, the direction was determined based on the bed orientation (S/D: strike and dip) and two-dimensional observations. The indirect measurement technique was applied to measurements taken in vertical sections (Phillips, 1977), with corrections applied when measurements were obtained from sections perpendicular to the flow direction (Dasgupta, 2002; Dott, 1973; Tucker, 2003), thus complementing the measurements of horizontal sections.

(2) Tables and wind-rose diagrams were prepared; and statistical methods were developed to obtain a resulting vector, which corresponds to the main paleocurrent direction, as well as subordinate directions. To restore the original directions of sediment dispersion prior to tectonic folding, all directional data measured in inclined strata were structurally corrected. At each sampling station, the orientation and dip of the local bedding plane (S_0) were systematically recorded, as well as the bearing and dip (or plunge) of the observed directional sedimentary structure.

The tectonic restoration was carried out using stereographic projection techniques with a Schmidt equal-area stereonet. The procedure consisted of rotating the local stratification plane back to the horizontal using its strike line as the axis of rotation, while vectorially dragging the corresponding directional indicator. For this purpose, kinematic algorithms of structural rotation in the Stereonet program (v.11) and the auxiliary software Stereo.win were used.

(3) The statistical analysis consisted of taking the azimuth arc from 0 to 180º, grouping the data into 20º intervals and entering them into a spreadsheet. As mentioned above, Schmidt's stereographic net methodology (Phillips, 1977; Steinmetz, 1962) was selected with statistical verification of the results, and the Stereo.win, Stereo.rar, and Stereonet programs were used to simplify the process. The comparison of traditional methods with software processing shows that the results are consistent. It is important to note that all measurements were corrected given the tectonic deformation observed in the field. In the case of the drag fold mentioned above, the bed orientation was rotated to the original position (N30W), and each measurement was analyzed individually and separately. It was observed that the corrected paleocurrents (94 measurements) allowed a more consistent geological interpretation (Figure 5).

(4) Assessment of model reliability: (a) reliability of the statistical models; (b) analysis of possible sources of error. Reliability is studied especially in the case of trough cross-stratification, separating eight stations in the Cuchilla Alta area. One source of error is the (not exact) correction itself, according to the variations in strike and dip due to the effects of tectonic deformation (Pamoukaghlián, 2012).

(5) Interpretation of provenance, paleoenvironment, and paleogeography.

Based on the facies analysis (Pamoukaghlián, 2012; Pamoukaghlián et al., 2014, 2021), a shallow marine paleoenvironment is interpreted, where it is expected that the analysis of paleocurrents of wave-generated asymmetric ripples yield random patterns. The paleocurrents measured from the trough cross-stratification could also

be variable. However, with more than 50 measurements, the sample is large enough to be considered in directional studies, according to the methodology described above (Pamoukaghlián, 2012; Tucker, 2003). In addition, the measurements of trough cross-stratification and planar cross-stratification (68 measurements in total for Cuchilla Alta) were analyzed together.

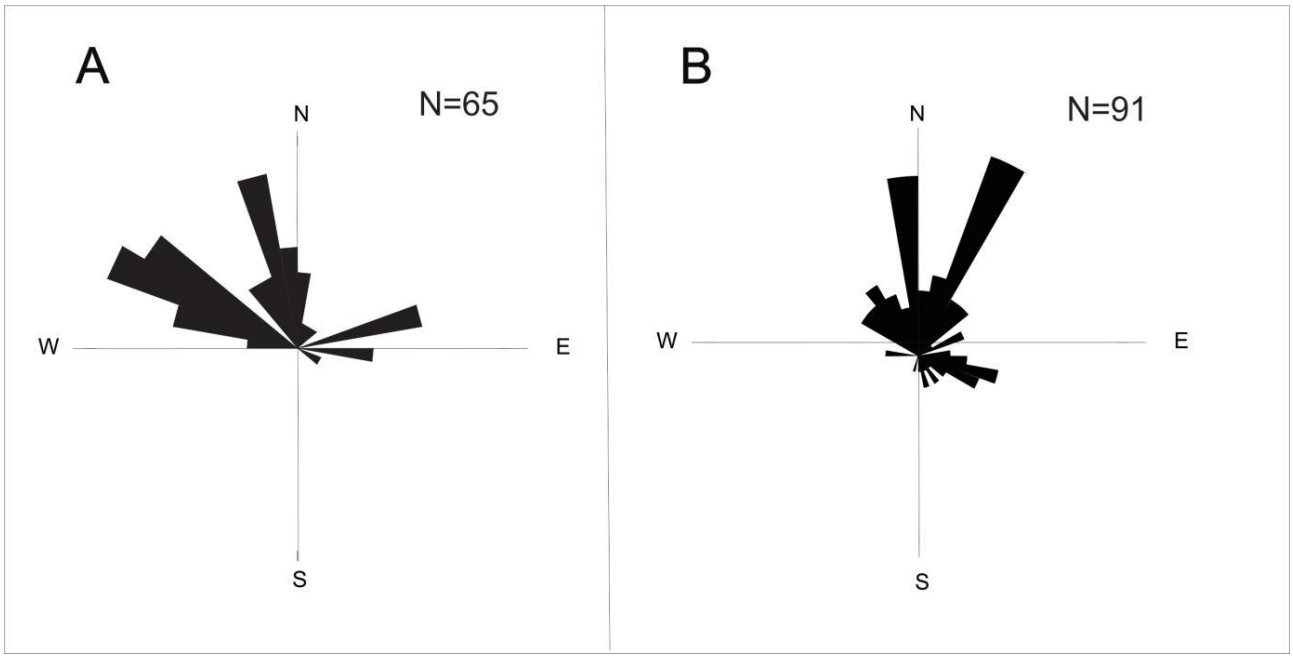


Figure 5. Paleocurrents measured in trough cross-stratification without tectonic correction (A) and with tectonic correction (B)

Note that the diagram on the right includes some measurements in planar cross-stratification.

4. Results

Paleocurrents are analyzed for the different sedimentary facies, with particular emphasis on the psammitic facies of the Cuchilla Alta Member, where the largest number of paleocurrents were measured. It is necessary to analyze separately the paleocurrents measured in the different sedimentary structures. The corresponding tables show the location, lithology, sedimentary structure, paleocurrent direction, and corrected direction for each measurement (Tables 1, 2, 3, 4, 5 and 6).

4.1 Paleocurrents in Psammitic Facies

The predominant directions for the Cuchilla Alta Member are towards the E and NE. The paleocurrents in the type area of Cuchilla Alta, based on measurements from planar and trough cross-stratification, present a predominant NE direction and a subordinate SE direction (Figures 7 and 8; Tables 1, 2, and 3). As mentioned above, each measured direction was corrected for the Cuchilla Alta area (94 data), as well as in other sectors of the coastal zone, according to the proposed methodology (Pamoukaghlián, 2012; Phillips, 1977; Steinmetz, 1962).

For the type area of the Cuchilla Alta Member, paleocurrents taken from asymmetric ripples, trough cross-stratification, and planar cross-stratification were measured (Tables 4 and 5). Paleocurrents from hummocky cross-stratification measurements were discarded because these should only be used as a last resort if available data are insufficient (Pamoukaghlián, 2012; Tucker, 1988). All directions were found to be predominantly toward the E.

Regarding trough cross bedding, excellent exposures of these sedimentary structures were observed in coarse to fine-grained sandstones, which can be seen in the coastal outcrops to the east of the study area, particularly in Cuchilla Alta (Figure 4D). A total of 56 measurements were taken at this locality (Tables 1, 2, and 3; Figure 7). Paleocurrents towards the NNE, E, and SE were measured (N30 to N150; Figure 7).

Interference ripple marks are excellent paleoenvironmental indicators; they are found in coastal paleoenvironments, evidencing orthogonal current directions (Figure 4A). Thus, they can be used to infer the coastline orientation and sediment-supply paleocurrents. In this case, the interference ripple marks indicate two perpendicular paleocurrent directions: SE (N140) and NE (N40).

Flute casts (PAF1, Figure 2) to the west of the outcrop area indicate paleocurrent directions to the NNE (Table 6, Figure 6). This paleocurrent direction corresponds to the main input direction (see Discussion).

Finally, parting lineation (Figure 4B) and cross-bedding of various types were observed (Figure 4). The parting lineation indicates a paleoslope descending towards the NNE (N10).

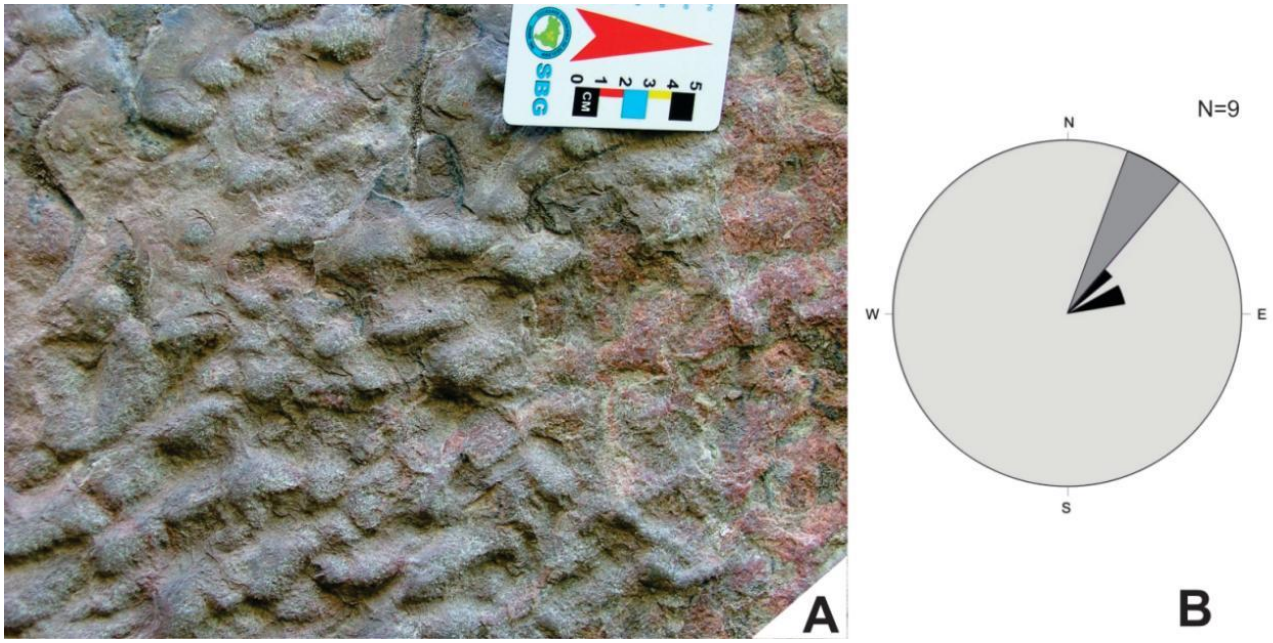


Figure 6. Flute casts in quartzarenites (A) with Rose Diagram of Paleocurrent Measurements (PAF1 in Figure 2)

4.2 Paleocurrents in Pelitic Facies

In the pelitic facies (siltstones and heterolithic siltstone-sandstone facies) of the Arroyo del Junquito Member, asymmetric ripples are observed as the only sedimentary structures where it is possible to measure paleocurrents. Although their directions are consistent with the general paleocurrent analysis (NNE and NE), these sedimentary structures cannot be taken into account in provenance analyses because wind and wave directions are highly variable, resulting in a distribution that is difficult to interpret.

Table 1. Paleocurrent data from the Cuchilla Alta Zone (PAF 40)

Lithology	*Bed orientation*	*Sedimentary structure*	*Paleocurrent measurement*	*Corrected measurement*
Quartzarenite	NS 20E	PCS	N20	350
Quartzarenite	NS20E	PCS	N20	350
Quartzarenite	EW, vertical	TCS	N20	80
Quartzarenite	EW, 55NW	TCS	N20	80
Quartzarenite	EW, vertical	TCS	N25	85
Quartzarenite	EW, vertical	TCS	N25	85
Quartzarenite	EW, vertical	PCS	N10W	50
Quartzarenite	EW, vertical	PCS	N75W	345
Quartzarenite	EW, vertical	PCS	N20W	40
Siltstone	EW, vertical	PCS	N90	150
Siltstone	EW, vertical	PCS	N90	150
Siltstone	EW, vertical	PCS	S	240
Siltstone	EW, vertical	PCS	N10	300
Siltstone	EW, vertical	PCS	N90	20
Siltstone	N25W, vertical	PCS	N25W	20
Siltstone	N25W, vertical	PCS	N	20
Siltstone	N25W, vertical	PCS	N	20
Quartzarenite	EW, vertical	PCS	N265	335
Quartzarenite	EW, vertical	HCS	N70	320
Quartzarenite	EW, vertical	PCS	N270	340
Quartzarenite	EW, vertical	PCS	N250	320
Quartzarenite	EW, vertical	PCS	N230	300
Quartzarenite	EW, vertical	PCS	N250	320
Quartzarenite	EW, vertical	PCS	N260	330
Quartzarenite	EW, vertical	TCS	N250	320
Coarse-grained sandstone	N65W, 45SW	TCS	N70	105
Coarse-grained sandstone	N65W, 45SW	TCS	N70	105
Coarse-grained sandstone	N65W, 45SW	TCS	N50	155
Coarse-grained sandstone	N65W, 45SW	TCS	N18W	17
Coarse-grained sandstone	N65W, 45SW	TCS	N70	105
Medium-grained sandstone	N50W, vertical	TCS	N	20
Medium-grained sandstone	N50W, vertical	TCS	N10W	10
Quartzarenite	N65,45SW	TCS	N15W	5
Quartzarenite	N65W, 45SW	TCS	N20W	360
Quartzarenite	N65W, 45SW	TCS	N60W	320
Quartzarenite	N65W, 45SW	TCS	N	20
Quartzarenite	N65W, 45SW	PCS	N10W	85

PCS: planar cross-stratification, TCS: trough cross-stratification.

Table 2. Paleocurrent data from the Cuchilla Alta Zone

Lithology	*Bed orientation*	*Sedimentary structure*	*Paleocurrent measurement*	*Corrected measurement*
Quartzarenite	N65W, 45SW	PCS	N15W	50
Quartzarenite	N65W, 45SW	TCS	N20W	60
Quartzarenite	N65W, 45SW	TCS	N60W	95
Quartzarenite	N65W, 45SW	PCS	N70	35
Quartzarenite	N65W, 45SW	TCS	N	125
Quartzarenite	N65W, 45SW	TCS	N90	350
Quartzarenite	N65W, 45SW	TCS	N15W	20
Quartzarenite	N65W, 45SW	TCS	N15W	25
Quartzarenite	N65W, 45SW	TCS	N10W	115
Quartzarenite	N65W, 45SW	TCS	N20W	85
Quartzarenite	N65W, 45SW	TCS	N50	120
Quartzarenite	N65W, 45SW	TCS	N25W	5
Quartzite	N50W, 90	TCS	N85	90
Quartzite	N50W, 90	TCS	N70	30
Quartzite	N50W, 90	TCS	N10	330
Quartzite	N50W, 90	TCS	N50W	350
Quartzite	N50W, 90	TCS	N30W	320
Quartzite	N50W, 90	TCS	N60W	305
Silty sandstone	N80W, 90	TCS	N75W	30
Silty sandstone	N80W, 90	TCS	N70W	100
Quartzite	N50W, 90	TCS	N90	110
Quartzite	N50W, 90	TCS	N	20
Quartzite	N50W, 90	TCS	N	20
Quartzite	N50W, 90	TCS	N10	40
Quartzite	N50W, 90	TCS	N30W	350
Quartzite	N50W, 90	TCS	N85	105
Quartzite	N50W, 90	TCS	N90	110
Quartzite	N50W, 90	TCS	N60W	320
Quartzite	N50W, 90	TCS	N65W	315
Silty arenite	N90, 72N	TCS	N65W	345
Silty arenite	N90, 72N	TCS	N65W	345
Silty arenite	N90, 72N	TCS	N60W	350
Silty arenite	N90, 72N	TCS	N65W	345
Silty arenite	N90, 72N	TCS	N65W	5
Subarkose	N65W, 70N	TCS	N85	175
Subarkose	N65W, 70N	PCS	N90	160
Subarkose	N65W, 70N	PCS	N75W	355
Subarkose	N65W, 70N	PCS	N120	190

Table 3. Paleocurrent data measured in planar cross-stratification (PCS) and trough cross-stratification (TCS) of the Cuchilla Alta Zone

Lithology	*Bed orientation*	*Sedimentary structure*	*Paleocurrent direction*	*Corrected measurement*
Subarkose	N90.72NE	PCS	N90	160
Subarkose	N90.72NE	PCS	N80W	355
Subarkose	N90.72NE	TCS	N65	135
Subarkose	N90.72NE	TCS	N70	140
Subarkose	N90.72NE	TCS	N50W	20
Subarkose	N90.72NE	TCS	N80W	350
Quartzarenite	N65W,70NE	TCS	N80W	310
Quartzarenite	N65W,70NE	TCS	N70	140
Quartzarenite	N65W,70NE	TCS	N50W	60
Quartzarenite	N65W,70NE	TCS	N50W	15
Quartzarenite	N65W,70NE	PCS	N80W	315
Quartzarenite	N65W,70NE	PCS	N5W	30
Quartzarenite	N65W,70NE	*HCS*	N10W	25
Quartzarenite	N65W,70NE	*HCS*	N90	60
Quartzarenite	N65W,70NE	PCS	N60W	335
Quartzarenite	N65W,70NE	PCS	N45W	350

Hummocky cross-stratification (HCS) measurements are excluded from the rose diagrams.

Table 4. Asymmetrical ripples of the type area of the Cuchilla Alta Member and the coastal area in Cuchilla Alta

Lithology	*Bed orientation*	*Sedimentary structure*	*Paleocurrent direction*
Sandstone	N30W, 45SW	Asymmetric ripples	N10
Sandstone	N30W, 45SW	Asymmetric ripples	N20
Sandstone	N30W, 45SW	Asymmetric ripples	N20
Sandstone	N30W, 45SW	Asymmetric ripples	N10
Sandstone	N30W, 45SW	Asymmetric ripples	N10W
Sandstone	N30W, 45SW	Asymmetric ripples	N340
Sandstone	N30W,43SW	Symmetrical ripples	N350
Pelites	N25W, 20-30SW	Asymmetric ripples	N10
Pelites	N25W, 20-30SW	Asymmetric ripples	N20W
Pelites	N25W, 20-30SW	Asymmetric ripples	N70W
Pelites	N25W, 20-30SW	Asymmetric ripples	N290
Pelites	N25W, 20-30SW	Asymmetric ripples	N270
Sandstone	N80, vertical	Asymmetric ripples	N135
Sandstone	N80, vertical	Asymmetric ripples	N135
Sandstone	N80, vertical	Asymmetric ripples	N75

Table 5. Paleocurrents measured in planar cross-stratification (PCS) in quartzarenites in the type area of the Cuchilla Alta Member

Bed orientation	*Sedimentary structure*	*Paleocurrent direction*
N30W, 45SW	PCS	N10
N30W, 45SW	PCS	N10
N30W, 45SW	PCS	N20
N30W, 45SW	PCS	N30
N30W, 45SW	PCS	N45
NS, 40W	PCS	N100
N30W, 45W	PCS	N30W
N30W, 45W	PCS	N60W
N30W, 45W	PCS	N80W

Table 6. Paleocurrent measurements from flute casts of the Cuchilla Alta Member at PAF 1 (Figure 2)

Bed orientation	*Lithology*	*Paleocurrent direction*
N25W, 40 SW	Quartzarenites	N20
N25W, 40 SW	Quartzarenites	N20
N25W, 40 SW	Quartzarenites	N30
N25W, 40 SW	Quartzarenites	N70
N25W, 40 SW	Quartzarenites	N20
N25W, 40 SW	Quartzarenites	N60
N30W, 55 SW	Quartzarenites	N30
N15W, 58 SW	Quartzarenites	N32
N15W, 58 SW	Quartzarenites	N40

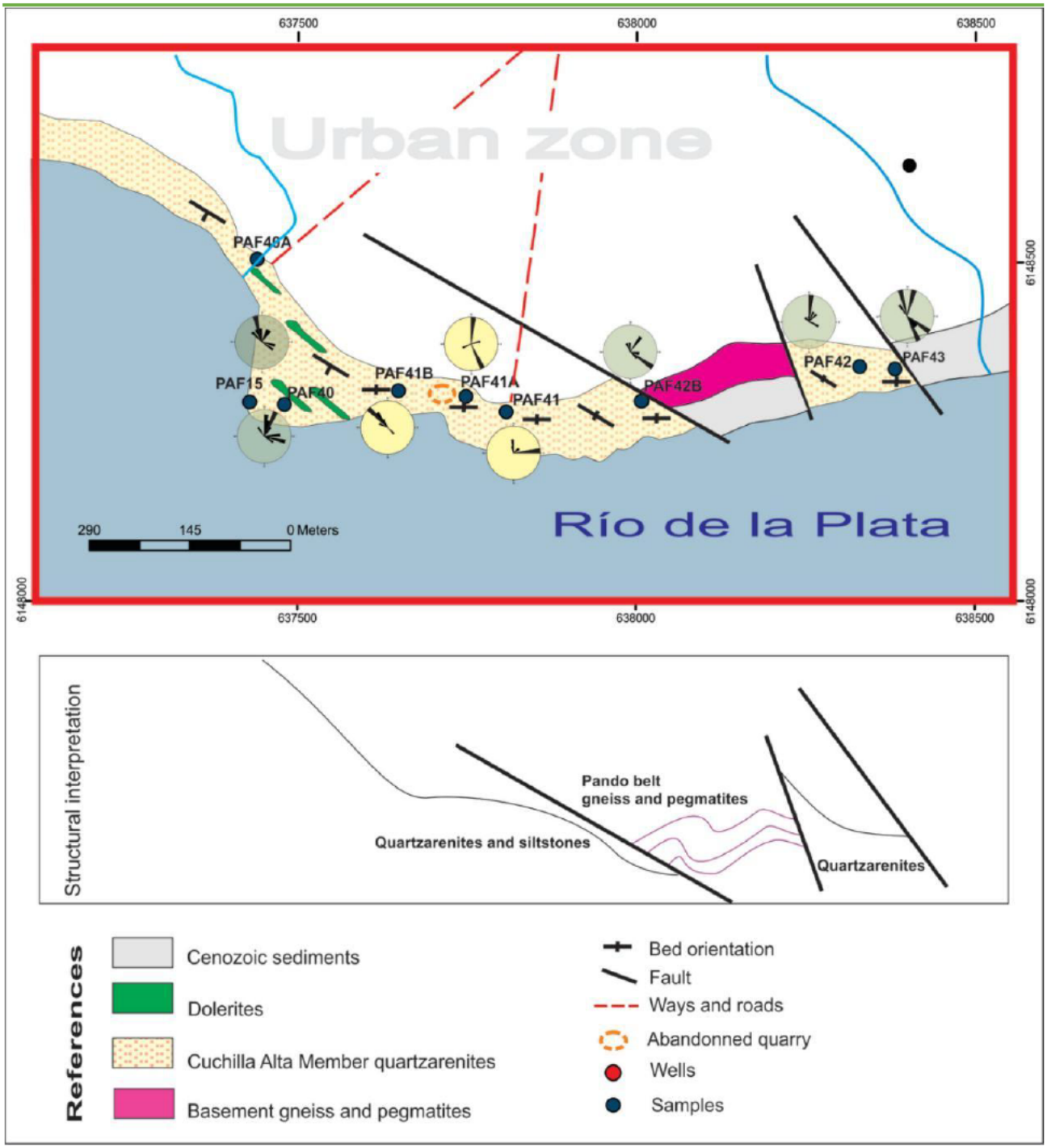


Figure 7. Geological map of the Cuchilla Alta area with location of paleocurrent diagrams and structural interpretation, including the identification of a large-scale drag fold

Note that the paleocurrents were corrected by rotating the bed orientation back to its original position (verified in the outcrops of the type area and other outcrop areas). The diagrams in yellow correspond to the abandoned quarry, whereas the gray-shaded diagrams correspond to the coastal outcrops of quartzarenites and siltstones.

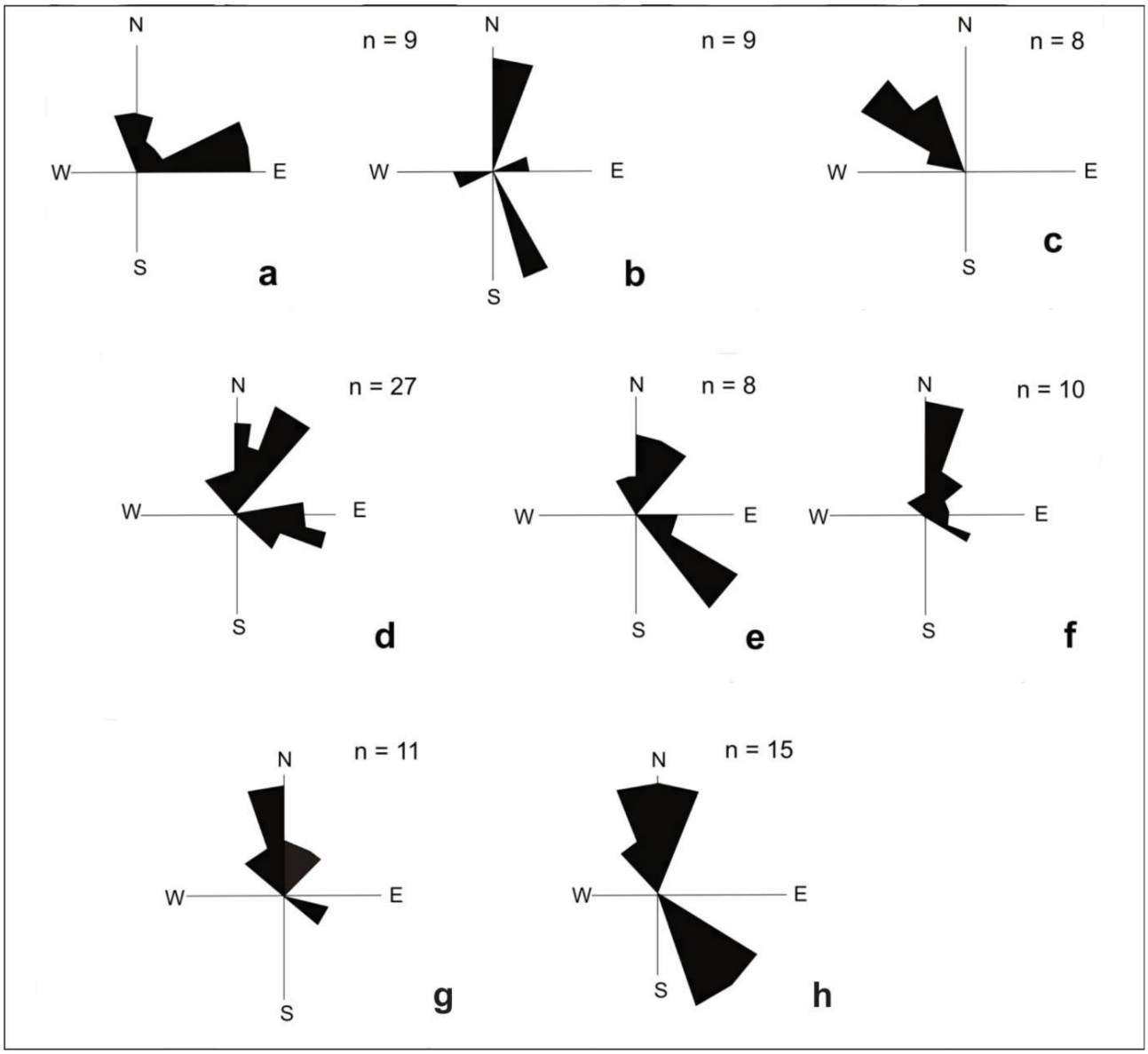


Figure 8. Paleocurrents in the Cuchilla Alta Zone: (a, b, c) paleocurrents measured in the Cuchilla Alta sandstone quarry; (d-h) in order corresponding to the locations from W to E on the map in Figure 7

Note that (a, b, c) present variable bimodal and unimodal patterns; while (d, e, f) present oblique patterns with a predominant paleocurrent towards the N and NE and a subordinate direction to the SE; they correspond to the area with the least deformation. Diagrams (g, h) correspond to the most highly deformed area and also present bimodal to oblique patterns with a predominant direction towards the N and subordinate direction to the SE.

5. Discussion

5.1 Interpretation of Paleocurrents, Paleogeography, and Tectonics

The paleocurrent analysis is presented below according to the sedimentary structures from which the measurements were obtained.

Interference ripple marks: Two perpendicular paleocurrents were obtained, one towards the SE (N140) and the other towards the NE (N40). The first is interpreted as a longshore current (linguoid ripples generated by ephemeral currents parallel to the coast), and the second would suggest a direction perpendicular to the coastline (asymmetrical ripples generated by waves; Pamoukaghlián et al., 2021), which is typical of a beach environment (Picard & High, 1970).

Paleocurrents measured from trough cross-stratification: An essentially bimodal pattern was obtained, with predominant paleocurrents to the NNE (dominant) and SE (subordinate), which is common in coastal marine environments (Miall, 2000; Reineck & Singh, 1980). A NNE paleocoast was interpreted (longshore drift) with the main sediment input coming from the W. The SE paleocurrents were interpreted as rip currents (Reineck & Singh, 1980). Only one isolated paleocurrent measurement toward the W was obtained. Coastal sandy environments are characterized by high variability (Miall, 2000; Reineck & Singh, 1980).

Measurements from flute casts: These are the most important provenance indicators because they show the direction of flow accurately (Selley, 2000). In this regard, a single measurement from these structures is more significant than several measurements in cross-bedding structures. Several data points from the same bed, together with another data point from a different bed in the same exposure, are statistically sufficient and can provide the paleocurrent direction with great precision (Dott, 1973; Nichols, 2009). However, flute casts are not good paleoenvironmental indicators, and it is necessary to complement them with other sedimentary structures to determine the environment in which they were formed, such as the interference ripple marks mentioned above (Pamoukaghlián et al., 2021). To this end, the different types of paleocurrents were studied separately (Tucker, 1988, 2003). In the specific case of the PAFm, paleocurrents towards the NNE were observed (Figure 6 and Table 6), evidencing provenance from the SSW.

Parting lineation: This sedimentary structure primarily indicates paleorelief and is a very good indicator of paleocurrent direction, but not of paleocurrent bearing (Miall, 2000; Picard & High, 1970). More specifically, it allows to infer the direction of the paleoslope, a paleogeographic feature (Selley, 2000). In other words, these structures are very useful to verify the direction, whereas the bearing of the paleocurrents must be confirmed from other sedimentary structures, such as flute casts (Miall, 2000). The quartz-arenites with parting lineation analyzed here (Figure 4B) indicate a paleoslope descending towards the NNE (N10), which verifies the measurements in the NNE-bearing flute casts.

In short, the paleocurrent analysis suggests a NNE-SSW to NW-SE coastline, with the basin deepening towards the eastern sector. The sediment contribution area was located to the W.

The paleocurrents of the Arroyo del Soldado Group (Nico Pérez Terrane) are also predominantly towards the east, including paleocurrents to the northeast (Gaucher, 2000). In the Sierras Bayas Group (Tandilia, Argentina), there is also evidence of paleocurrents to the east, according to reported trough cross-bedding measurements (Poiré, 1987), although that overall paleocurrent pattern is different because it occupies a different paleogeographic position (the southern edge of the craton; Ballivián Justiniano et al., 2020; Gaucher et al., 2008). The analysis of paleocurrents alone is not sufficient evidence to interpret the provenance of sedimentary rocks. However, when combined with U-Pb isotopic data in detrital zircons, Sm-Nd in associated pelites, and sandstone petrography, the results are consistent and together provide clear and compelling evidence. Sandstone petrography shows a provenance from an interior craton to recycled orogen (Pamoukaghlián et al., 2021). This recycled orogen can be identified by the ages of detrital zircons and their Hf isotopic ratios of the three aforementioned units, with a significant Mesoproterozoic population in all three cases (Finney & Gaucher, 2022; Gaucher et al., 2008). The Mesoproterozoic orogen in question is identified as a proto-Andean belt located west of the Río de la Plata Craton (Finney & Gaucher, 2022; Gaucher et al., 2008, 2009, 2011; Santos et al., 2008). Nd model ages show the same pattern: Paleoproterozoic values of 2.5-2.0 Ga typical of the craton and Mesoproterozoic model ages of 1.55 Ga from the erosion of the proto-Andean belt (Pamoukaghlián et al., 2021). In other words, complementing the paleocurrent data with other lines of evidence confirms a source area to the west, identified with the Río de la Plata Craton (*sensu* Bossi & Cingolani, 2009).

Field observations and paleocurrent results show the existence of a drag fold at the eastern end of the PAFm outcrop area. The eastern region is characterized by a change in the strike and dip of the beds, which shift from

the regional strike N45W to N65W in Araminda-Biarritz (Figure 2) and then to E-W to the east of Cuchilla Alta (Figures 2 and 8). The outcrops further east also show greater deformation than the rest of the unit (Pamoukaghlián, 2012). Likewise, the paleocurrents of the eastern area show a rotation similar to that verified in the direction of the beds: once corrected, they yield values consistent with those from the rest of the formation (Figure 8). The obvious cause of the identified drag fold is the Sarandí del Yi Shear Zone, which outcrops a few km E of the easternmost PAFm outcrops (Spoturno et al., 2004) and had its last movement (sinistral reactivation) in the Ediacaran-Cambrian (Gaucher et al., 2008; Oriolo et al., 2015). The main dextral movement of this megashear, responsible for the curvature of the Florida Dike Swarm (Figure 1; Bossi & Campal, 1992; Bossi & Ferrando, 2001), took place in the Mesoproterozoic and, therefore, is not recorded by the PAFm (Gaucher et al., 2021; Teixeira et al., 1999).

5.2 Paleoenvironment

The results obtained contribute to the paleoenvironment and paleogeographic analyses of the PAFm within the context of the Río de la Plata Craton, according to a reconstruction of the PAFm paleoenvironment and its associated paleocurrents. Regarding the paleoenvironmental evidence obtained, the most notable findings are the paleocurrents measured from interference ripple marks. These are diagnostic of a beach paleoenvironment (Tucker, 2003), which is consistent with lithostratigraphic evidence and the analysis of sedimentary facies (Pamoukaghlián, 2012; Pamoukaghlián et al., 2014, 2021).

The sedimentary structures and paleocurrent pattern observed corroborate what Pamoukaghlián (2012) proposed regarding the type of platform, which would have been dominated by storms and, secondarily, waves (*sensu* Posamentier & Walker, 2006). The importance of storms is evidenced by the frequent occurrence of hummocky cross-stratification, which is more frequent in the upper part of the Cuchilla Alta Member (Figure 3). Some of the structures observed at point PAF32 (Figure 2) have extreme wavelengths of up to 7 m (Figure 4E). Since the outcrop is located at the boundary between the Cuchilla Alta and Arroyo del Junquito members, it is possible that the deeper paleobathymetry (compared to the base of the Cuchilla Alta Member, Figure 4C) favored greater wavelengths, as recorded in current environments (Yang et al., 2006). On the other hand, these extreme values suggest the occurrence of hurricanes capable of generating large waves, which are more typical of warm periods and tropical environments (Ito et al., 2001; Qi et al., 2023). A tropical environment for upper PAFm is suggested by sandstone petrography and clay mineral association (Pamoukaghlián et al., 2021), the occurrence of carbonates in the Arroyo de la Tuna Member, and the significant carbonate thicknesses (up to 900 m) in the correlative units in Uruguay and Argentina (e.g. Gaucher et al., 2004; Gómez-Peral et al., 2017).

5.3 Sedimentary Structures and Hydrogeology

Sedimentary structures are conditioning factors for porosity and, above all, for the permeability of clastic sedimentary formations (Hossain et al., 2024; Huysmans et al., 2008). As a first approximation, the predominant control of permeability for the PAFm are diagenetic processes and specifically sandstone cementation (Pamoukaghlián, 2012), which has led to considering the PAFm as a fractured aquifer rather than a porous one (M. Aboy et al., personal communication, 2022; Aboy et al., 2022). The lower part of the Yerbal Formation (Arroyo del Soldado Group), a correlative unit of the PAFm (Poiré & Gaucher, 2009), also behaves as a fractured aquifer of medium productivity (Gaucher et al., 2023). Moreover, it is known that the composition and diagenetic processes in sandy formations are controlled by sedimentary provenance (e.g. Zhang et al., 2025). The new paleocurrent data make it possible to begin investigating the influence of provenance on permeability in the specific case of the PAFm, given that, as established above, the source areas were located to the W. One possible approach would be to study the variations in the porosity of the levels of coarse-grained sandstones at the base of the Cuchilla Alta Member, potentially the most permeable, in W-E (proximal-distal) transects. This line of research therefore remains open, complementary to the study of the areas where the PAFm behaves as

a fractured aquifer (M. Aboy et al., personal communication; 2022). This could provide a geological basis for further groundwater exploration in the PAFm, for irrigation and drinking-water supply in a water-deficient area (M. Aboy et al., personal communication, 2022).

6. Conclusions

According to the results obtained, the main findings of the paleocurrent analysis of the PAFm indicate that the predominant paleocurrent directions are to the NNE and SE, according to the paleocurrents measured, respectively, in planar and trough cross-stratification and verified by the paleocurrent direction indicated by flute casts (NNE). Therefore, the main sediment contribution is interpreted to come from emerged areas located to the W. A source area located to the W, in the Río de la Plata Craton, is consistent with independent evidence such as U-Pb ages of detrital zircons, Nd model ages in pelites, Hf model ages, and sandstone petrography for the PAFm (Finney & Gaucher, 2022; Gaucher et al., 2008; Pamoukaghlián et al., 2021).

At the regional scale, the Arroyo del Soldado Group (Nico Pérez Terrane) presents predominant paleocurrent directions to the east, as does the Piedras de Afilar Formation (Tandilia Terrane). The Sierras Bayas Group (Tandilia Terrane) presents predominant paleocurrent directions to the south because it occupies a different paleogeographic position. Therefore, the paleocurrent directions provide further evidence of provenance from the west for the aforementioned Neoproterozoic units. It is confirmed that the source of Mesoproterozoic zircons for the PAFm and correlative units was a hypothetical proto-Andean belt (e.g. Gaucher et al., 2011), which must have been located at the western edge of the Río de la Plata Craton. This belt is identified as the counterpart of the Grenvillian Orogen of Laurentia (Finney & Gaucher, 2022; Santos et al., 2008).

The results obtained provide a basis for guiding studies of sedimentary facies variations along proximal-distal (W-E) profiles. These studies could help determine whether there are areas less affected by the later diagenetic processes that reduced the porosity and permeability of the PAFm sandstones and, consequently, their potential as a porous aquifer. So far, the observed hydrogeological behavior for the PAFm sandstones is that of a fractured aquifer, due to the pervasive silicification that affects them.

Acknowledgments

To the colleagues at the Centro de Investigaciones Geológicas, where this research was developed, especially to Dr. Lucía Gómez Peral and in memory of Dr. Jorge Bossi, for his companionship during field trips, leaving behind his unmistakable legacy and teachings.

Transparency of Data

Available data: The entire data set that supports the results of this study was published in the article itself.

Author Contribution Statement

	K Pamoukaghlián	C Gaucher	D Poiré
Conceptualization	■	■	■
Investigation	■		
Writing – original draft	■		
Writing – review and editing	■	■	■

References

Aboy, M., Masquelin, H., & Pamoukaghlián, K. (2022). Análisis estructural e hidrogeológico de la Formación Piedras de Afilar (Neoproterozoico Superior) – Canelones. In *XII Jornada Geociencias: Libro de resúmenes* (p. 13). PEDECIBA Geociencias. https://www.pedeciba.edu.uy/admin/uploads/estatico/Libro%20de%20res%C3%BAmenes%20JGEO22.pdf

Abre, P., Bossi, J., Cingolani, C., Gaucher, C., Piñeyro, D., & Blanco, G. (2014). El terreno Tandilia en Uruguay y Argentina. In J. Bossi & C. Gaucher (Eds.), *Geología del Uruguay: Tomo 1. Predevónico* (pp. 89-119). Polo.

Arrouy, M. J., Gaucher, C., Poiré, D. G., Xiao, S., Gómez-Peral, L. E., Warren, L. V., Bykova, N., & Quaglio, F. (2019). A new record of late Ediacaran acritarchs from La Providencia Group (Tandilia System, Argentina) and its biostratigraphical significance. *Journal of South American Earth Sciences, 93*, 283-293. https://doi.org/10.1016/j.jsames.2019.05.015

Ballivián Justiniano, C. A., Basei, M. A. S., Sato, A. M., González, P. D., Benítez, M. E., & Lanfranchini, M. E. (2020). The Neoproterozoic basement of the Sauce Chico Inlier (Ventania System): Geochemistry and U–Pb geochronology of igneous rocks with African lineage in central-eastern Argentina. *Journal of South American Earth Sciences, 98*, Article 102391. https://doi.org/10.1016/j.jsames.2019.102391

Basei, M. A. S., Sánchez Bettucci, L., Peel, E., & Preciozzi, F. (2016). LAICPMS U–Pb zircon ages from basement and metamorphic cover of Piedra Alta Terrane, Rio de la Plata Craton, Uruguay. In C. Gaucher & J. Montaño (Eds.), *VIII Congreso Uruguayo de Geología: Actas* (p. 117). Sociedad Uruguaya de Geología. https://drive.google.com/file/d/1_CJ6HqO5JNYGYxGaqlwBiJBqlEAnkIM0/view

Bossi, J., & Campal, N. (1992). Magmatismo y tectónica transcurrente durante el Paleozoico inferior en Uruguay. In J. C. Gutiérrez Marco, J. Saavedra, & I. Rábano (Eds.), *Paleozoico inferior de Ibero-América* (pp. 343-356). Universidad de Extremadura.

Bossi, J., & Cingolani, C. A. (2009). Extension and general evolution of the Río de la Plata Craton. In C. Gaucher, A. N. Sial, G. P. Halverson, & H. E. Frimmel (Eds.), *Neoproterozoic-Cambrian tectonics, global change and evolution: A focus on southwestern Gondwana* (pp. 73-85). Elsevier. https://doi.org/10.1016/S0166-2635(09)01604-1

Bossi, J., & Ferrando, L. (2001). *Carta geológica del Uruguay a escala 1/500.000: Versión digital 2.0*. Universidad de la República.

Bossi, J., Ferrando, L., Montaña, J., Campal, N., Morales, N., Gancio, F., Schipilov, A., Piñeyro, D., & Sprechmann, P. (1998). *Carta geológica del Uruguay: Escala 1/500.000*. Universidad de la República.

Bossi, J., & Gaucher, C. (2004). The Cuchilla Dionisio Terrane, Uruguay: An allochthonous block accreted in the Cambrian to SW-Gondwana. *Gondwana Research, 7*(3), 661-674. https://doi.org/10.1016/S1342-937X(05)71054-6

Bossi, J., & Navarro, R. (1991). *Geología del Uruguay*. Universidad de la República.

Bossi, J., & Piñeyro, D. (2014). Terreno Piedra Alta. In J. Bossi & C. Gaucher (Eds.), *Geología del Uruguay: Tomo 1. Predevónico* (pp. 45-86). Polo.

Bossi, J., Piñeyro, D., & Cingolani, C. (2005). El límite del Terreno Piedra Alta (Uruguay): Importancia de la faja milonítica sinestral de Colonia. In *Actas XVI Congreso Geológico Argentino* (pp. 173-180). Asociación Geológica Argentina.

Bossi, J., Preciozzi, F., & Campal, N. (1993). *Predevoniano en el Uruguay: Tomo 1. Terreno Piedra Alta*. Ministerio de Industria y Energía.

Chernicoff, C. J., Zappettini, E. O., Santos, J. O. S., Godeas, M. C., Belousova, E., & McNaughton, N. J. (2012). Identification and isotopic studies of early Cambrian magmatism (El Carancho Igneous Complex) at the boundary between Pampia terrane and the Río de la Plata craton, La Pampa province, Argentina. *Gondwana Research, 21*(2-3), 378-393. https://doi.org/10.1016/j.gr.2011.04.007

Cingolani, C. A. (2011). The Tandilia System of Argentina as a southern extension of the Río de la Plata craton: An overview. *International Journal of Earth Sciences, 100*, 221-242. https://doi.org/10.1007/s00531-010-0611-5

Cingolani, C. A., Bossi, J., Varela, R., & Navarro, R. (1990). Nuevos datos geológicos y geocronológicos del macizo granítico de Cerro Colorado, Florida, Uruguay. In *Resúmenes ampliados del Primer Congreso Uruguayo de Geología* (Vol. 1, p. 101-105). Sociedad Uruguaya de Geología. https://drive.google.com/file/d/16ziurU-Zn9ZAR0cl8vrJDmTJS-BjhR4j/view

Coronel, N., Oyhantçabal, P., & Sportuno, J. (1982). Consideraciones estructurales de la Formación Piedras de Afilar en su área tipo, en los alrededores de la estación de Piedras de Afilar, Depto. de Canelones, Uruguay. In *Actas del 5o Congreso Latinoamericano de Geología* (pp. 48-60). El Congreso.

Dasgupta, P. (2002). Determination of paleocurrent direction from oblique sections of trough cross-stratification: A precise approach. *Journal of Sedimentary Research, 72*(1), 217-219. https://doi.org/10.1306/050401720217

Dott, R. H., Jr. (1973). Paleocurrent analysis of trough cross stratification. *Journal of Sedimentary Research, 43*(3), 779-783. https://doi.org/10.1306/74D72865-2B21-11D7-8648000102C1865D

Dristas, J. A., Masquelin, H., Wemmer, K., Bianchi, F. D., Martínez, J. C., & Massonne, H.-J. (2023). New insights into the Piedra de Afilar Formation, Canelones department of Uruguay: Very-low-grade metamorphism, pressure solution, and age. *Journal of South American Earth Sciences, 123*, Article 104237. https://doi.org/10.1016/j.jsames.2023.104237

Finney, S. C., & Gaucher, C. (2022). Hf isotopes in detrital zircon point to a Mesoproterozoic orogenic belt bordering the western margin of the Río de la Plata Craton. *The Journal of Geology, 130*(1), 1-22. https://doi.org/10.1086/717889

Gaucher, C. (2000). Sedimentology, palaeontology and stratigraphy of the Arroyo del Soldado Group (Vendian to Cambrian, Uruguay). *Beringeria*, *26*, 5-120.

Gaucher, C. (2014). Grupo Arroyo del Soldado. In J. Bossi & C. Gaucher (Eds.), *Geología del Uruguay: Tomo 1. Predevónico* (pp. 313-339). Polo.

Gaucher, C. (2018). The Ediacaran–Early Cambrian fossil record in Southwest Gondwana. In S. Siegesmund, M. A. S. Basei, P. Oyhantçabal, & S. Oriolo (Eds.), *Geology of Southwest Gondwana* (pp. 543-560). Springer. https://doi.org/10.1007/978-3-319-68920-3_20

Gaucher, C., Boggiani, P. C., Sprechmann, P., Sial, A. N., & Fairchild, T. R. (2003). Integrated correlation of the Vendian to Cambrian Arroyo del Soldado and Corumbá Groups (Uruguay and Brazil): Palaeogeographic, palaeoclimatic and palaeobiologic implications. *Precambrian Research, 120*(3-4), 241-278. https://doi.org/10.1016/S0301-9268(02)00140-7

Gaucher, C., Collazo, M. P., Reolón, G., Akerman, F., & Álvarez, P. (2023). Subdivisión litoestratigráfica de la Formación Yerbal (Ediacárico, Uruguay) y aspectos hidrogeológicos. In *Actas de las Primeras Jornadas de Geología y Minería Jorge Bossi* (pp. 25-26). Universidad de la República.

Gaucher, C., Finney, S. C., Poiré, D. G., Valencia, V. A., Grove, M., Blanco, G., Pamoukaghlián, K., & Gómez Peral, L. (2008). Detrital zircon ages of Neoproterozoic sedimentary successions in Uruguay and Argentina: Insights into the geological evolution of the Río de la Plata Craton. *Precambrian Research, 167*, 150-170. https://doi.org/10.1016/j.precamres.2008.07.006

Gaucher, C., Frei, R., Chemale, F., Jr., Frei, D., Bossi, J., Martínez, G., Chiglino, L., & Cernuschi, F. (2011). Mesoproterozoic evolution of the Río de la Plata Craton in Uruguay: At the heart of Rodinia? *International Journal of Earth Sciences, 100*, 273-288. https://doi.org/10.1007/s00531-010-0562-x

Gaucher, C., Frei, R., Samaniego, L., Will, T. M., Chemale, F., Gargiulo, M. F., Poiré, D. G., Ling, X., Li, X., & Li, Q. (2021). The Tapes Complex (Nico Pérez Terrane, Uruguay): Constraining the Mesoproterozoic evolution of the Río de la Plata Craton. *Journal of South American Earth Sciences, 105*, Article 102906. https://doi.org/10.1016/j.jsames.2020.102906

Gaucher, C., Frimmel, H. E., & Germs, G. J. B. (2009). Tectonic events and palaeogeographic evolution of southwestern Gondwana in the Neoproterozoic and Cambrian. In C. Gaucher, A. N. Sial, G. P. Halverson, & H. E. Frimmel (Eds.), *Neoproterozoic-Cambrian tectonics, global change and evolution: A focus on southwestern Gondwana* (pp. 295-316). Elsevier. https://doi.org/10.1016/S0166-2635(09)01621-1

Gaucher, C., Poiré, D. G., Gómez Peral, L. E., & Chiglino, L. (2005). Litoestratigrafía, bioestratigrafía y correlaciones de las sucesiones sedimentarias del Neoproterozoico-Cámbrico del Cratón del Río de la Plata (Uruguay y Argentina). *Latin American Journal of Sedimentology and Basin Analysis, 12*(2), 145-160. https://www.scielo.org.ar/scielo.php?script=sci_arttext&pid=S1851-49792005000200006

Gaucher, C., Sial, A. N., Blanco, G., & Sprechmann, P. (2004). Chemostratigraphy of the lower Arroyo del Soldado Group (Vendian, Uruguay) and palaeoclimatic implications. *Gondwana Research, 7*(3), 715-730. https://doi.org/10.1016/S1342-937X(05)71058-3

Gaucher, C., & Sprechmann, P. (1999). Upper Vendian skeletal fauna of the Arroyo del Soldado Group, Uruguay. *Beringeria, 23*, 55-91.

Gaucher, C., Will, T., Pamoukaghlián, K., & Ling, X. X. (2026). Dolerites of the Piedras de Afilar Formation (Uruguay): U–Pb age, inheritance and insights for the Tandilia Terrane. In E. Peel (Ed.), *XIV South American Symposium on Isotope Geology: Book of abstracts* (pp. 80-81). Sociedad Uruguaya de Geología. https://drive.google.com/file/d/1v5HB8t6tKoP0DaIk5AgptT2Ze7gYoXdi/view

Gómez-Peral, L. E., Kaufman, A. J., Arrouy, M. J., Richiano, S., Sial, A. N., Poiré, D. G., & Ferreira, V. P. (2018). Preglacial palaeoenvironmental evolution of the Ediacaran Loma Negra Formation, far southwestern Gondwana, Argentina. *Precambrian Research, 315*, 120-137. https://doi.org/10.1016/j.precamres.2018.07.005

Gómez-Peral, L. E., Sial, A. N., Arrouy, M. J., Richiano, S., Ferreira, V. P., Kaufman, A. J., & Poiré, D. G. (2017). Paleo-climatic and paleo-environmental evolution of the Neoproterozoic basal sedimentary cover on the Río de La Plata Craton, Argentina: Insights from the $\delta^{13}C$ chemostratigraphy. *Sedimentary Geology, 353*, 139-157. https://doi.org/10.1016/j.sedgeo.2017.03.007

Halverson, G. P., Hoffman, P. F., Schrag, D. P., Maloof, A. C., & Rice, A. H. N. (2005). Toward a Neoproterozoic composite carbon-isotope record. *Geological Society of America Bulletin, 117*(9-10), 1181-1207. https://doi.org/10.1130/B25630.1

Hartmann, L. A., Campal, N., Santos, J. O. S., McNaughton, N. J., Bossi, J., Schipilov, A., & Lafon, J.-M. (2001). Archean crust in the Rio de la Plata Craton, Uruguay: SHRIMP U–Pb zircon reconnaissance geochronology. *Journal of South American Earth Sciences, 14*(6), 557-570. https://doi.org/10.1016/S0895-9811(01)00055-4

Hossain, S., Hampson, G. J., Jacquemyn, C., Jackson, M. D., & Chiarella, D. (2024). Permeability characterisation of sedimentological facies in the Bunter Sandstone Formation, Endurance CO_2 storage site, offshore UK. *International Journal of Greenhouse Gas Control, 135*, Article 104140. https://doi.org/10.1016/j.ijggc.2024.104140

Huysmans, M., Peeters, L., Moermans, G., & Dassargues, A. (2008). Relating small-scale sedimentary structures and permeability in a cross-bedded aquifer. *Journal of Hydrology, 361*, 41-51. https://doi.org/10.1016/j.jhydrol.2008.07.047

Ito, M., Ishigaki, A., Nishikawa, T., & Saito, T. (2001). Temporal variation in the wavelength of hummocky cross-stratification: Implications for storm intensity through Mesozoic and Cenozoic. *Geology, 29*(1), 87-89. https://doi.org/10.1130/0091-7613(2001)029<0087:TVITWO>2.0.CO;2

Jones, G. H. (1956). Memoria explicativa y mapa geológico de la región oriental del departamento de Canelones. *Boletín del Instituto Geológico del Uruguay*, (34), 1-193.

Lenz, C., Fernandes, L. A. D., McNaughton, N. J., Porcher, C. C., & Masquelin, H. (2011). U–Pb SHRIMP ages for the Cerro Bori Orthogneisses, Dom Feliciano Belt in Uruguay: Evidences of a ~800 Ma magmatic and ~650 Ma metamorphic event. *Precambrian Research, 185*(3-4), 149-163. https://doi.org/10.1016/j.precamres.2011.01.007

Miall, A. D. (2000). *Principles of sedimentary basin analysis* (3rd ed.). Springer. https://doi.org/10.1007/978-3-662-03999-1

Nichols, G. (2009). *Sedimentology and stratigraphy* (2nd ed.). Wiley-Blackwell.

Oriolo, S., Oyhantçabal, P., Heidelbach, F., Wemmer, K., & Siegesmund, S. (2015). Structural evolution of the Sarandí del Yí Shear Zone, Uruguay: Kinematics, deformation conditions and tectonic significance. *International Journal of Earth Sciences, 104*, 1759-1777. https://doi.org/10.1007/s00531-015-1166-2

Oyhantçabal, P., Derrégibus, M. T., Muzio, R., & Nardi, L. V. S. (1998). The Soca intrusion: A rapakivi granite of Uruguay. *Journal of South American Earth Sciences, 11*(2), 169-178. https://doi.org/10.1016/S0895-9811(98)00008-X

Oyhantçabal, P., Siegesmund, S., Wemmer, K., & Passchier, C. W. (2011). The transpressional connection between Dom Feliciano and Kaoko Belts at 580–550 Ma. *International Journal of Earth Sciences, 100*, 379-390. https://doi.org/10.1007/s00531-010-0577-3

Oyhantçabal, P., Spoturno, J., Aubet, N., Cazaux, S., & Huelmo, S. (2003). Proterozoico del suroeste del Uruguay: Nueva propuesta estratigráfica para la formación Montevideo y el magmatismo asociado. *Revista de la Sociedad Uruguaya de Geología*, (Publicación Especial nº 1), 38-48.

Pamoukaghlián, K. (2012). *Sedimentología y estratigrafía de la formación Piedras de Afilar, Terreno Tandilia, Uruguay* [Doctoral dissertation, Universidad Nacional de La Plata]. SEDICI. https://doi.org/10.35537/10915/29586

Pamoukaghlián, K., Gaucher, C., Bossi, J., Sial, A. N., & Poiré, D. G. (2006). First C and O isotopic data for the Piedras de Afilar Formation (Tandilia Terrane, Uruguay): Their bearing on its correlation and age. In *V South American Symposium on Isotope Geology: Short papers* (pp. 277-283). Talleres Idea Gráfica.

Pamoukaghlián, K., Gaucher, C., Frei, R., Poiré, D. G., Chemale, F., Frei, D., & Will, T. M. (2017). U-Pb age constraints for the La Tuna Granite and Montevideo Formation (Paleoproterozoic, Uruguay): Unravelling the structure of the Río de la Plata Craton. *Journal of South American Earth Sciences, 79*, 443-458. https://doi.org/10.1016/j.jsames.2017.09.004

Pamoukaghlián, K., Gaucher, C., & Poiré, D. G. (2010). Nueva propuesta litoestratigráfica para la Formación Piedras de Afilar, Neoproterozoico Superior de Uruguay. In *V Congreso Uruguayo de Geología: II Simposio Internacional del Neoproterozoico de la Cuenca del Plata*. Sociedad Uruguaya de Gología. https://drive.google.com/file/d/11ghr8hXfxuNLzRfGE-1YomvOc0fSMSsf/view

Pamoukaghlián, K., Gaucher, C., Poiré, D. G., & Frei, R. (2021). The Piedras de Afilar Formation (Neoproterozoic, Uruguay): Sedimentology and provenance of a key unit for SW-Gondwana paleogeography. *Journal of South American Earth Sciences, 108*, Article 103176. https://doi.org/10.1016/j.jsames.2021.103176

Pamoukaghlián, K., Poiré, D. G., & Gaucher, C. (2014). Piedras de Afilar. In J. Bossi & C. Gaucher (Eds.), *Geología del Uruguay: Tomo 1. Predevónico* (pp. 121-138). Polo.

Pecoits, E., Gingras, M., Aubet, N., & Konhauser, K. (2008). Ediacaran in Uruguay: Palaeoclimatic and palaeobiological implications. *Sedimentology, 55*(3), 689-719. https://doi.org/10.1111/j.1365-3091.2007.00918.x

Phillips, F. C. (1977). *La aplicación de la proyección estereográfica en geología estructural*. Blume.

Picard, M. D., & High, L. R. (1970). Interference ripple marks formed by ephemeral streams. *Journal of Sedimentary Petrology, 40*(2), 708-711. https://doi.org/10.1306/74D7201D-2B21-11D7-8648000102C1865D

Poiré, D. G. (1987). *Mineralogía y sedimentología de la formación Sierras Bayas en el núcleo septentrional de las sierras homónimas, partido de Olavarría, Provincia de Buenos Aires* [Doctoral dissertation, Universidad Nacional de La Plata]. SEDICI. http://sedici.unlp.edu.ar/handle/10915/4742

Poiré, D. G., & Gaucher, C. (2009). Lithostratigraphy. In C. Gaucher, A. N. Sial, G. P. Halverson, & H. E. Frimmel (Eds.), *Neoproterozoic-Cambrian tectonics, global change and evolution: A focus on southwestern Gondwana* (pp. 87-101). Elsevier. https://doi.org/10.1016/S0166-2635(09)01605-3

Posamentier, H. W., & Walker, R. G. (Eds.). (2006). *Facies models revisited.* SEPM. https://doi.org/10.2110/pec.06.84

Preciozzi, F., Basei, M. A., & Masquelin, H. (1999). New geochronological data from the Piedra Alta Terrane (Rio de la Plata Craton). In *II Simposio Sudamericano de Geología Isotópica = II South American Symrosium on Isotope Geology: Actas* (pp. 341-344). Segmar.

Qi, L., Hou, M., Cawood, P. A., Lang, X., Zhu, S., & Zhang, M. (2023). Neoproterozoic storm deposits in western Yangtze: Implications for the sea conditions during the middle Sturtian glaciation. *Precambrian Research, 384*, Article 106945. https://doi.org/10.1016/j.precamres.2022.106945

Reineck, H.-E., & Singh, I. B. (1980). *Depositional sedimentary environments: With reference to terrigenous clastics* (2nd rev. and updated ed.). Springer-Verlag. https://doi.org/10.1007/978-3-642-81498-3

Ribot, A. M., Bossi, J., Cingolani, C., & Piñeyro, D. (2005). Caracterización petrográfica y cinemática de la faja milonítica Colonia–Arroyo Pavón en el sur del Terreno Piedra Alta, Uruguay: Zona de cizalla principal en basamento precámbrico. In *Actas del XVI Congreso Geológico Argentino* (pp. 457-464). Asociación Geológica Argentina.

Santos, J. O. S., Chernicoff, C. J., Zappettini, E. O., McNaughton, N. J., & Greau, Y. (2017). U-Pb geochronology of Martín García, Sola, and Dos Hermanas Islands (Argentina and Uruguay): Unveiling Rhyacian, Statherian, Ectasian, and Stenian of a forgotten area of the Río de la Plata Craton. *Journal of South American Earth Sciences, 80*, 207-228. https://doi.org/10.1016/j.jsames.2017.09.029

Santos, J. O. S., Hartmann, L. A., Bossi, J., Campal, N., Schipilov, A., Piñeyro, D., & McNaughton, N. J. (2003). Duration of the Trans-Amazonian Cycle and its correlation within South America based on U-Pb SHRIMP geochronology of the La Plata Craton, Uruguay. *International Geology Review, 45*(1), 27-48. https://doi.org/10.2747/0020-6814.45.1.27

Santos, J. O. S., Rizzotto, G. J., Potter, P. E., McNaughton, N. J., Matos, R. S., Hartmann, L. A., Chemale, F., Jr., & Quadros, M. E. S. (2008). Age and autochthonous evolution of the Sunsás Orogen in West Amazon Craton based on mapping and U–Pb geochronology. *Precambrian Research, 165*(3-4), 120-152. https://doi.org/10.1016/j.precamres.2008.06.009

Selley, R. C. (2000). *Applied sedimentology* (2nd ed.). Academic Press.

Spoturno, L., Oyhantçabal, P., Goso, C., Aubet, N., Cazaux, S., Huelmo, S., & Morales, E. (2004). *Mapa geológico y de recursos minerales del departamento de Canelones a escala 1:100.000: Memoria explicativa*. Universidad de la República; MIEM.

Steinmetz, R. (1962). Analysis of vectorial data. *Journal of Sedimentary Petrology, 32*(4), 801-812. https://doi.org/10.1306/74D70D76-2B21-11D7-8648000102C1865D

Teixeira, W., Renne, P. R., Bossi, J., Campal, N., & D'Agrella Filho, M. S. (1999). ^{40}Ar–^{39}Ar and Rb–Sr geochronology of the Uruguayan dike swarm, Río de la Plata Craton and implications for Proterozoic intraplate activity in western Gondwana. *Precambrian Research, 93*(2), 153-180. https://doi.org/10.1016/S0301-9268(98)00087-4

Tucker, M. E. (Ed.). (1988). *Techniques in sedimentology*. Blackwell Scientific Publications.

Tucker, M. E. (2003). *Sedimentary rocks in the field: A practical guide* (3rd ed.). John Wiley & Sons.

Walther, K. (1948). El basamento cristalino de Montevideo: Relaciones con yacimientos análogos del Uruguay y de países vecinos. *Boletín del Instituto Geológico del Uruguay,* (33), 1-138.

Will, T. M., Gaucher, C., Frimmel, H. E., Ling, X.-X., Shi, W., Li, X.-H., & Li, Q.-L. (2023). Ediacaran to Cambrian tectonomagmatic events in the Southern Dom Feliciano Belt, Uruguay: From a plate margin to an intraplate setting and the assembly of SW Gondwana. *Gondwana Research, 115*, 155-182. https://doi.org/10.1016/j.gr.2022.12.004

Will, T. M., Gaucher, C., Ling, X.-X., Li, X.-H., Li, Q.-L., & Frimmel, H. E. (2019). Neoproterozoic magmatic and metamorphic events in the Cuchilla Dionisio Terrane, Uruguay, and possible correlations across the South Atlantic. *Precambrian Research, 320*, 303-322. https://doi.org/10.1016/j.precamres.2018.11.004

Yang, B., Dalrymple, R. W., & Chun, S. (2006). The significance of hummocky cross-stratification (HCS) wavelengths: Evidence from an open-coast tidal flat, South Korea. *Journal of Sedimentary Research, 76*(1), 2-8. https://doi.org/10.2110/jsr.2006.01

Zhang, Q., Yang, C., Gu, Y., Tian, Y., Liu, H., Xiao, W., Wang, Z., & Mi, Z. (2025). Microscopic pore-throat structure and fluid mobility of tight sandstone reservoirs in multi-provenance systems, Triassic Yanchang Formation, Jiyuan area, Ordos Basin. *Energy Geoscience, 6*(2), Article 100407. https://doi.org/10.1016/j.engeos.2025.100407